Eur. J. Mineral.
1990, **2**, 427-449

Relaxation in silicate melts

DONALD B. DINGWELL and SHARON L. WEBB

Bayerisches Geoinstitut, Universität Bayreuth, Postfach 10 12 51, D-8580 Bayreuth, F.R.G.

Abstract: The glass transition is a kinetic barrier that divides the behavior of silicate melts into two types, liquid and glassy. Liquid behavior is the equilibrium response of a melt to an applied perturbation, resulting in the determination of an equilibrium liquid property. The equilibrium may be stable (superliquidus) or metastable (subliquidus). Glassy behavior occurs when the timescale of the perturbation is too short for melt equilibration. This can occur when the frequency of an applied sinusoidal perturbation is too high or when the observation time of an experiment is too short. The time- or frequency-dependent response of the structure and properties of a melt to a perturbation is termed relaxation. Liquid and glassy behavior are relaxed and unrelaxed behavior, respectively.

Linear viscoelastic theory provides mechanical models for the prediction of the isothermal transition from liquid to glassy behavior. A simple series combination of Hookean spring and Newtonian dashpot (a Maxwell element) is capable of predicting the timescale corresponding to the glass transition from the ratio of the relaxed viscosity to the infinite frequency elastic modulus. We review some experimental work on silicate melts that can be used to constrain the location of the glass transition in time-temperature space at 1 atm pressure (e.g., ultrasonic wave propagation, fiber elongation, torsional testing, scanning calorimetry).

The microscopic origin of the glass transition in silicate melts is related to the exchange of Si-O bonds. Recent ^{29}Si NMR work indicates that the Si-O bond exchange frequency matches the timescale of the glass transition. This explains the Newtonian viscosity of silicate liquids. No extended species (e.g., "polymers") can exist at higher temperatures and longer timescales than the lifetime of the fundamental Si-O bond. Silicate melts, however, become non-Newtonian as the strain rate approaches the equilibration rate of the Si-O bonds. Such a correlation between Si-O bond exchange and the viscous flow mechanism, in turn, explains the success of the Eyring relationship in relating high temperature oxygen and silicon self-diffusion to viscosity.

Knowledge of the structural relaxation timescale is important in extracting equilibrium information from studies of the structure and properties of quenched glasses. Quench rate-dependent speciation data for glasses imply a temperature-dependence of the species equilibrium in the liquid state. Estimation of the relaxation times associated with the quench rates allows reconstruction of the temperature-dependence of homogeneous equilibria in liquids.

Experimental work on silicate melts should consider the location of the experimental method in time-temperature space, with respect to the glass transition. Diffusivity measurements, for example, are influenced by the glass transition. When the duration of a diffusivity experiment crosses the volume relaxation time, an inflection in the temperature-dependence of diffusivity of cations is observed. A second "transition" in diffusivity behavior is expected to occur at higher temperatures when the diffusivity of network oxygen and silicon approaches that of other cations.

Key-words: structural relaxation, viscosity, diffusivity, speciation, non-Newtonian, quench rate, silicate melt, liquid, glass.

1. Introduction

The glass transition has been described as "that phenomenon... in which a solid amorphous phase exhibits with changing temperature a more or less sudden change in the derivative thermodynamic properties such as heat capacity and thermal expansivity from crystal-like to liquid-like values" (Wong & Angell, 1976). The development of frequency domain methods for experimental

0935-1221/90/0002-0427 $ 5.75

determination of physical properties (e.g. ultrasonic inteferometry, a.c. calorimetry) has demonstrated that such behavior characterizing the glass transition may also be observed at constant temperature by varying the frequency of observation (Tauke *et al.*, 1968; Birge, 1986). Frequency domain observations of the glass transition can probe the frequency-dependence of the relaxation of various structural elements of an equilibrium melt structure at a single temperature. In contrast, the temperature-dependence of melt properties near the glass transition result from the relaxation of structural elements of the melt superimposed upon the temperature-dependence of the equilibrium configurational state. The generalization of these features defining the glass transition in temperature-time space are the subject of this paper.

The key to understanding the dynamics of silicate melts lies in the determination of the response or relaxation time of macroscopic and microscopic melt properties. The glass transition represents the highest temperature relaxation process observed in silicate melts. Above the glass transition (at longer times and higher temperatures) the silicate melt is a true liquid in equilibrium with, and "instantaneously" (i.e., faster than the observation timescale) responding to, perturbations in stress, temperature and electrical fields (section 1.).

Recent, careful observations of the "freezing out" of structural degrees of freedom across the glass transition have begun to yield a mechanistic description of the processes responsible for structural relaxation (section 2.).

A knowledge of the thermal history of glass permits the estimation of the "fictive" or last equilibration temperature of the liquid during cooling. Such data, combined with quench rate-dependent glass property data, yield estimates of the temperature-dependence of the liquid structure or property (section 3.).

By measuring physical properties across the glass transition it is possible to model disequilibrium behavior of natural melts during igneous processes and experimental studies (section 4.).

The glass transition has an influence on most physical properties of silicate melts. In order to understand the observed physical properties of a melt in any given experiment, two timescales must be considered, the experimental dwell time (τ_d) and the inverse of the probe frequency (τ_p) (section 5.).

2. The glass transition

2.1. Viscoelasticity

Fig. 1 is a representation of the glass transition in temperature-time space. The line divides the dynamic behavior of silicate melts into two fields of response; a liquid field at long timescales and high temperatures and a glass field at short timescales and low temperatures. The response of silicate melts in the liquid field is termed "relaxed" and the response in the glass field is termed "unrelaxed". The glass transition "temperature" varies with the timescale of the laboratory measurement but the relatively restricted timescale range (10 to 1000 sec) of most classical (calorimetric, dilatometric) determinations of the glass transition temperature (T_g) has made it useful to define a single glass transition temperature for most practical considerations in glass-making.

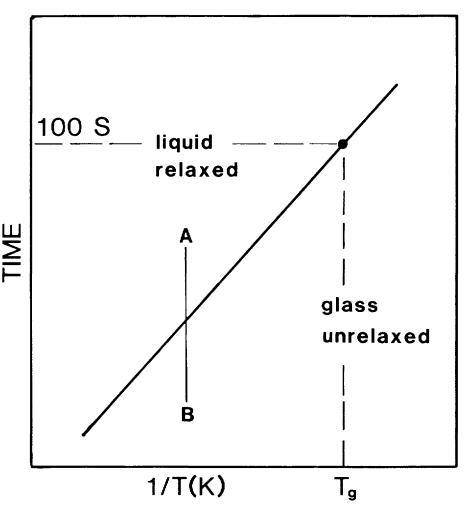

Fig. 1. The glass transition in temperature-time space. The liquid and glass fields are defined as relaxed and unrelaxed, respectively. The vertical section A—B across the glass transition is illustrated in Fig. 2. The glass transition line is the locus of mean relaxation times at varying temperature.

The glass transition is, on closer inspection, a region of mixed, relaxed and unrelaxed, or "partially relaxed" behavior. An isothermal section through the glass transition curve is illustrated in Fig. 2 with the example of stress — strain behavior. If a sinusoidal perturbation of the shear stress

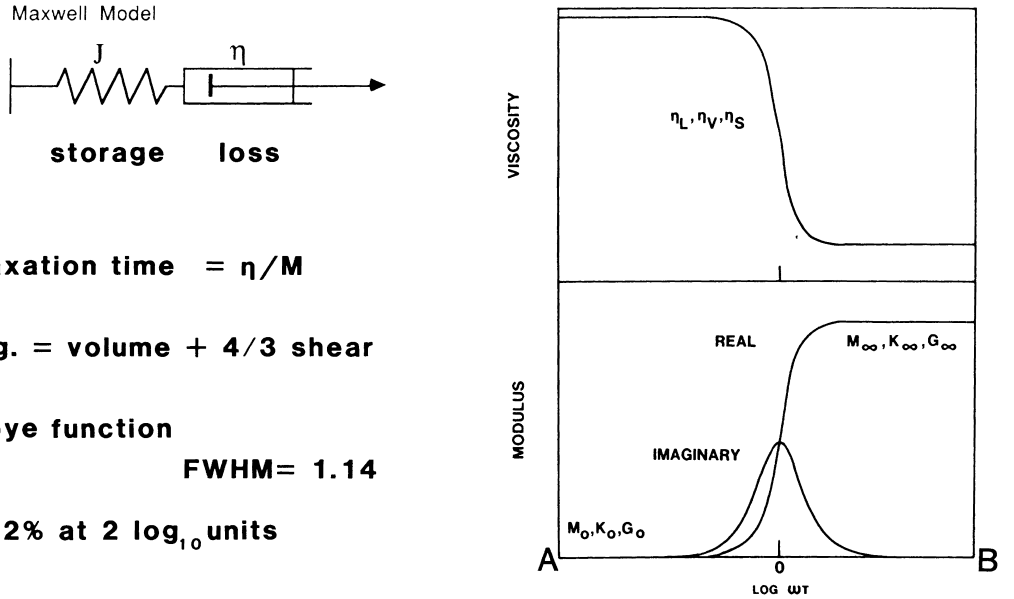

Fig. 2. Calculated frequency-dependent behavior of longitudinal, volume and shear viscosities (η_L, η_V and η_S, respectively) and moduli (M, K and G, respectively) of a linear viscoelastic material with a relaxation time, τ, plotted as a function of $\omega\tau$, where ω is the angular frequency of the applied sinusoidal stress. The subscripts "0" and "∞" indicate zero frequency and infinite frequency values.

field is applied to a silicate melt near the glass transition then the strain response recorded will be a mixture of viscous dissipation or "loss", and elastic "storage", of strain energy. Alternatively, the response of melt properties (e.g., volume) resulting from a step function in the external conditions (e.g., stress) consists of three segments: an instantaneous, elastic segment, a delayed, recoverable component and a delayed non-recoverable, viscous component. In both cases, (frequency domain or time domain) the proportions of energy storage and loss can be described in terms of mechanical components which model the macroscopic linear viscoelastic behavior of the melt. The simplest mechanical model of linear viscoelasticity (Maxwell, 1867) is a series combination of a viscous dashpot with Newtonian viscosity η and a Hookean spring with elastic modulus M (or its inverse, compliance J). The components are illustrated in Fig. 2. The relaxation timescale (τ) defining the glass transition curve in Fig. 1 corresponds to the timescale calculated from the ratio of Newtonian viscosity to infinite frequency elastic modulus.

$$\tau = \eta / M_\infty \qquad (1)$$

In Fig. 2, the viscoelastic behavior in the vicinity of the relaxation time is illustrated in terms of the phase shift ($\varphi(\omega)$) of measured strain ($\varepsilon^*(\omega)$) with respect to applied sinusoidal stress ($\sigma^*(\omega)$) by plotting real (M′) and imaginary (M″) components of the modulus across the glass transition, where

$$M(\omega) \exp i\varphi(\omega) = M'(\omega) + iM''(\omega) = \sigma^*(\omega) / \varepsilon^*(\omega), \qquad (2)$$

(Kampfmann & Berckhemer, 1985). The maximum of the imaginary component and the inflection in the real component of the modulus correspond to the mean relaxation time. For the Maxwell element, the relaxation function (M″) is described by a Debye function with a full width at half maximum of 1.14 $\log_{10}$ units of time (or frequency).

Fig. 3 illustrates that the real behavior of silicate melts is more complex than that described by the Maxwell model. Fig. 3a presents the results of Mills (1974) for torsional stress relaxation in a sodium trisilicate glass. The frequency of the applied sinusoidal torsional stress was varied and the resulting phase shift of strain was recorded. The resulting distribution of real and imaginary components of the shear modulus (G′ and G″, respectively) indicate a significant broadening of the vis-

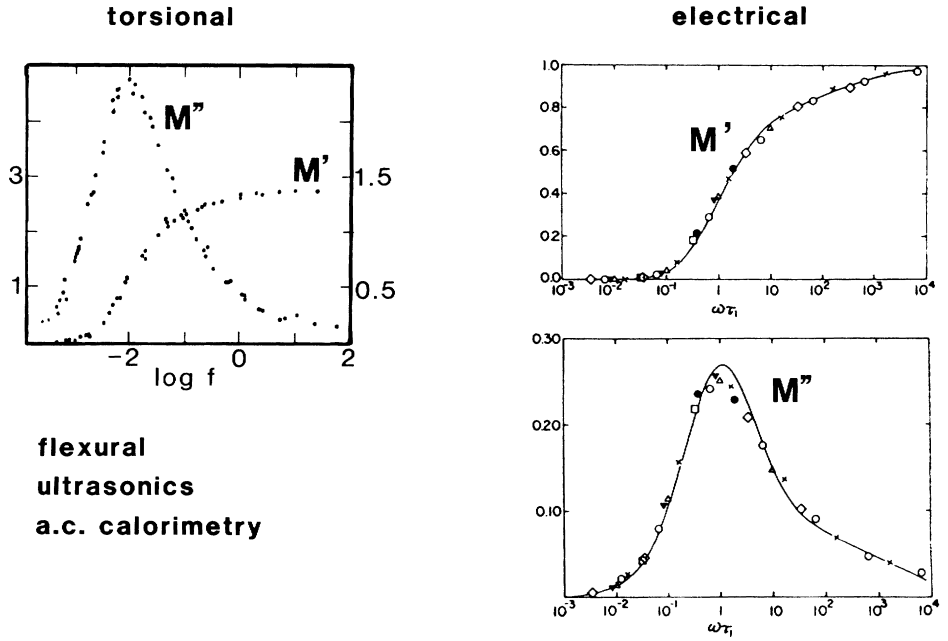

Fig. 3. The real and imaginary components of the shear (torsional) and electrical moduli for sodium trisilicate melt. Torsional data from Mills (1974) (M′ in units of 10^{11} dyne/cm^2, M″ in units of 10^{10} dyne/cm^2) and normalized electric modulus data from Provenzano *et al.* (1972).

coelastic region and a distinct asymmetry skewed towards higher frequency, compared with the Maxwell model. These two features of stress relaxation have been observed in numerous relaxation studies of silicate and non-silicate materials and appear to be a general feature of the relaxation process, unrelated to chemistry. Fig. 3b illustrates the same general features for the electrical modulus obtained from electrical field relaxation studies in sodium trisilicate glass (Provenzano *et al.*, 1972). Other examples of frequency domain investigations of relaxation include flexural, ultrasonic (Tauke *et al.*, 1968) and a.c. calorimetric (Birge, 1986) techniques. In each case the structural relaxation of the sample is recorded from the observation of a different physical property such as heat capacity, elastic modulus or electrical conductivity.

One additional feature of stress relaxation in silicate melts is illustrated in Fig. 4 where the viscosity determined by longitudinal acoustic wave propagation (Rivers & Carmichael, 1987) is compared with the shear viscosity determined from concentric cylinder viscometry (see references in Rivers & Carmichael, 1987). The longitudinal viscosity is related to the shear viscosity by

$$\eta_L = \eta_V + (4/3)\eta_S \qquad (3)$$

where η_L, η_V and η_S are the longitudinal, volume and shear viscosities, respectively. If we set the shear and volume viscosities to be equal, then the solid line in Fig. 4 is the expected result. The

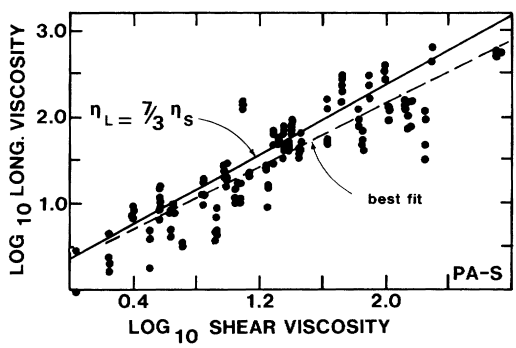

Fig. 4. The relationship between longitudinal and shear viscosities in silicate melts. The solid line represents the correlation predicted from the assumption that the volume and shear viscosities are equal. The dashed line is the best fit from a least squares regression and lies within 1σ of the theoretical line. The longitudinal data are from Rivers & Carmichael (1987) and the shear data are from references therein. (Reproduced from Dingwell & Webb, 1989a.)

dashed curve of Fig. 4 represents the best fit to the available data which lies within error of the solid curve (Dingwell & Webb, 1989a). This equivalence of the shear and volume viscosities combined with data for the shear and volume (or bulk) moduli (see below), permits the comparison of volume and shear relaxation studies.

2.2. τ curves

The shear viscosity of silicate melts ranges over several orders of magnitude with temperature and with composition (e.g., Fig. 1 of Richet, 1984). In contrast, the value of the shear modulus is relatively constant at $\log_{10} G_\infty$ (Pa) $= 10 \pm 0.5$ (Bansal & Doremus, 1986; Bucaro & Dardy, 1974). The Maxwell relationship (Eqn. (1)) thus illustrates that the shear viscosity of a silicate melt is a near linear measure of the shear relaxation time for the melt (Angell, 1984; Angell, 1988; Angell & Torrell, 1983). Values of the shear relaxation time of several silicate melts, calculated using Eqn. (1) and setting $\log_{10} G_\infty$ (Pa) $= 10$, are illustrated in Fig. 5 in temperature-time space. It can be seen from Fig. 5 that the range of relaxation times corresponding to the glass transition for each silicate melt composition is very large. SiO_2 melt has the longest relaxation time at any temperature, while sodium disilicate has very short relaxation times. Some of the curves cross with decreasing temperature and the curvature can vary significantly, indicating that the temperature-dependence of structural relaxation is relatively complex. As noted above, the glass transition "temperature" of each melt composition occurs approximately where the τ curves of Fig. 5 cross the range of 10 to 1000 s. Thus the glass transition temperature of SiO_2, obtained using experimental methods in the time range of 10 to 1000 s, occurs at $\cong$ 1100 °C whereas that of sodium disilicate occurs at $\cong$ 450 °C. The glass transition temperatures obtained from Fig. 5 at 10–1000 s should and do correspond to T_g data from scanning calorimetry (Martens *et al.*, 1987) and dilatometry (Richet, 1984). These τ curves record the timescale of measurements required to observe the glass transition at a specific temperature. For example ultrasonic measurements at timescales of 10^{-7} s record a glass transition of 840 °C for sodium disilicate whereas torsion measurements at a timescale of 1 s record the glass transition at 500 °C.

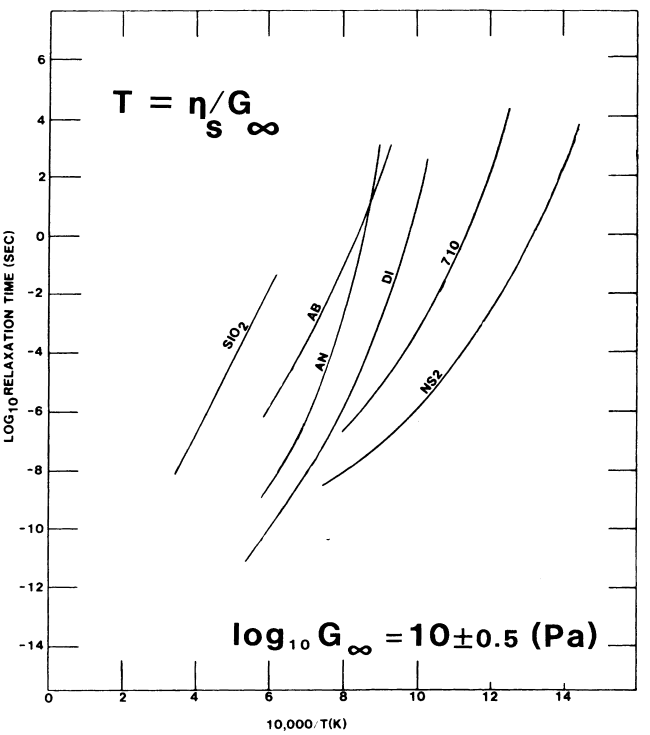

Fig. 5. The liquid-glass transition as a function of temperature plotted for several silicate melts calculated from Eqn. (1). The viscosity data used are from references in Richet (1984), for SiO_2, AB-albite, AN-anorthite, DI-diopside: Astin (1962: 710-soda lime SRM 710). (Redrawn from Dingwell & Webb, 1989a.)

2.3. Atomistic origin

The self diffusivity of oxygen in silicate melts has been correlated with shear viscosity through the Stokes-Einstein and Eyring equations (Glasstone *et al.*, 1941; Dunn, 1982; Shimizu & Kushiro, 1984). The Eyring equation is:

$$D = kT/\eta\lambda \qquad (4)$$

for D, k, T, η and λ, the oxygen diffusivity, Boltzmann's constant, temperature (K), viscosity and the diffusive jump length, respectively.

Shimizu & Kushiro (1984) have plotted shear viscosity versus oxygen diffusivity for a number of melt compositions. Their Fig. 2 (redrawn in Fig. 6) indicates calculated viscosities that are close to the Eyring prediction for an oxygen atom as the diffusing unit. When the longitudinal viscosity (2.33 η_s) is substituted for shear viscosity (η_s) in the comparison of Shimizu & Kushiro (1984) the data are within error of the prediction of Eqn. (4), using a diffusing species diameter of 2.8×10^{-10} m. This supports the proposal that the basic unit of viscous flow is the diffusive jump of O^{2-}.

The Eyring equation fails for oxygen in SiO_2. The calculated diffusivities for the Si-O bond breaking mechanism using Eqn. (4) (viscosity data from Hofmaier & Urbain, 1968) are up to 3 orders of magnitude slower than oxygen diffusivities measured using isotopic gas permeation or exchange methods (Sucov, 1963; Williams, 1965; Muehlenbachs & Schaeffer, 1977). This may be explained by the proposal (e.g., Muehlenbachs & Schaeffer) that these experiments involve transport of physically dissolved O_2 gas. This interpretation is consistent with the low activation energy ($\sim$ 20 kcal mole^{-1}) for the process (Muehlenbachs & Schaeffer, 1977; Schaeffer & Muehlenbachs, 1978; Schaeffer, 1984). The Eyring equation predicts the diffusivity of Si in silicate melts (see Fig. 19). It is possible that the Eyring equation will predict the timescale of O diffusion in SiO_2 in the absence of physically dissolved O_2 gas.

Further information on the basic viscous flow process comes from high-temperature static ^{29}Si NMR work of Liu *et al.* (1988). They have studied the static ^{29}Si NMR spectrum of $Na_2Si_2O_5$ melt as a function of temperature (Fig. 7). At low temperature they observed a distribution of Q species including Q_2, Q_3 and Q_4. At temperatures near 650 °C the distinction of Q species was lost and a single time-averaged position of the Q species was obtained. At temperatures near the loss of resolution of the Q species, Liu *et al.* (1988) have used the resonant frequency difference between Q species as an estimate of the rate of exchange. We have plotted the range for their estimate of the timescale of Q species exchange in Fig. 7. It falls within error of the τ curve for $Na_2Si_2O_5$. This is consistent with the idea that the ex-

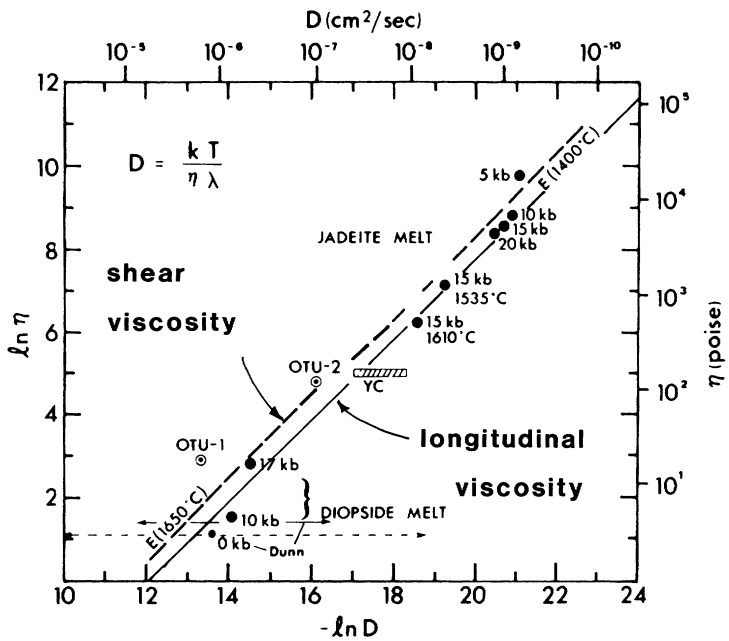

Fig. 6. The Eyring relationship for silicate melts. (Redrawn from Shimizu & Kushiro, 1984.)

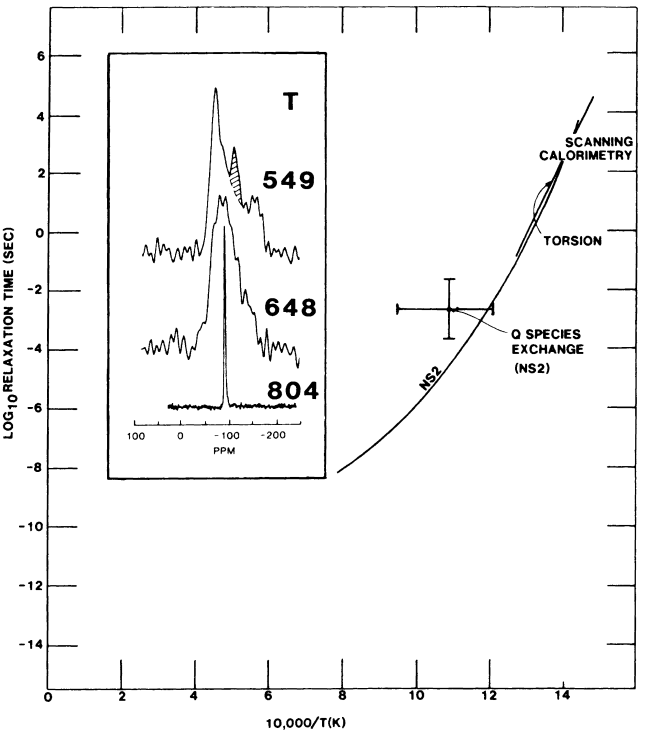

Fig. 7. Location of the glass transition using ^{29}Si T_2 (spin-spin) relaxation times from the nuclear magnetic resonance study of Liu *et al.* (1988). The loss of species distinction across the glass transition is consistent with Si-O bond exchange at the timescale of structural relaxation. Also plotted are the torsional data of Mills (1974). (Inset redrawn from Liu *et al.*, 1988.)

change of oxygens between Si atoms is the origin of the glass transition. More recent, better data and lineshape simulations on $K_2Si_4O_9$ liquid confirm this behavior (Farnan & Stebbins, 1990). These results indicate that it should be possible to study the temperature-dependence of the structure of relaxed silicate melts using high-temperature NMR. The experiments must be performed at temperatures high enough to accomplish structural relaxation on a reasonable dwell timescale (τ_d, see section 5.2) but low enough to maintain bond exchange frequencies lower than the NMR probe frequency (τ_p, see section 5.3). This should be possible for a reasonable temperature range, for example, for $Na_2Si_2O_5$ melt.

3. Quench rates

3.1. q curves

Data obtained on glasses cannot be used to predict liquid behavior without an understanding of the kinetic barrier separating the two, i.e., the glass transition. Given a quench rate-dependence of the glass transition, however, the quench rate may be used as the independent variable in indirect studies (on glasses) of the temperature-dependence of the liquid structure. A large number of microscopic (e.g., Infrared, Raman, NMR, Mössbauer) and macroscopic (density, heat capacity, thermal conductivity, mass and thermal diffusivity) investigations of glasses have been performed in an effort to constrain the structure and behavior of silicate liquids that form the dominant component of igneous processes. Few of the studies reported in the geological literature, however, contain a treatment of the glass transition in interpreting the data. As a result, one potentially important aspect of liquid structure, i.e., its temperature-dependence, is very poorly constrained. Below we illustrate that the glass transition can be controlled, by varying quench rate, to yield information on the temperature-dependence of liquid structure and properties. The method is based on recent estimations of the quench rate-, temperature- and composition-dependence of the fictive or equilibration temperature of silicate melts (Scherer, 1984; Dingwell & Webb, 1989 a,b).

One of the earliest models of the glass transition was presented by Tool & Eichlin (1931) who proposed that a single parameter, in addition to the number normally required to define the equilibrium state of the system (via the phase rule), could be specified, in order to predict glass properties. The single "rate" parameter proposed was termed the "fictive" temperature of the glass. If the timescale of relaxation or equilibration of a glass were single-valued then the fictive temperature concept would predict glass properties exactly. In practice, this is not so and thus modifications to the original fictive temperature concept were subsequently found to be required for glasses with complicated thermal histories (Ritland, 1954) and for the description of the relaxation process in detail (e.g., Kurkjian, 1963; Narayanaswamy, 1971) and far from equilibrium (Scherer, 1986). The fictive temperature concept however, remains valuable in predicting liquid properties from glass data (Moynihan *et al.*, 1976; Narayanaswamy, 1988) and is an important first step towards characterizing the temperature of equilibration recorded by a glass structure.

The significance of quench rates in experimental studies of liquid silicates can be illustrated in time-temperature space. Fig. 8 is a schematic plot of time versus reciprocal absolute temperature. The upward curving line represents the glass transition between equilibrated, liquid properties (at long timescales and high temperatures) and unequilibrated, glass properties (at short timescales and low temperatures). An experiment performed by holding a melt at a dwell temperature for a certain time is represented in Fig. 8 as a point in time-temperature space. In order to achieve equilibration, the dwell point of an experiment must lie on the high-temperature, long timescale side of the τ curve for the composition being studied.

The equilibration time pertaining to a given quench rate is a constant, independent of temperature (Ritland 1954; Moynihan *et al.*, 1976; Scherer, 1986). The locus of points defining the equilibration time at the glass transition, obtained during a single quench rate, defines a horizontal line in Fig. 8. These quench lines may be termed "q" curves. It is the relationship between the (1) experimental dwell point, (2) quench (q) curve and (3) glass transition (τ) curve which determines the fictive or true equilibration temperature of glass properties dependent on the configuration or mobility of oxygens, measured in quench glasses. It is the intersection of the q and τ curves that yields the value of the relaxation time at the glass

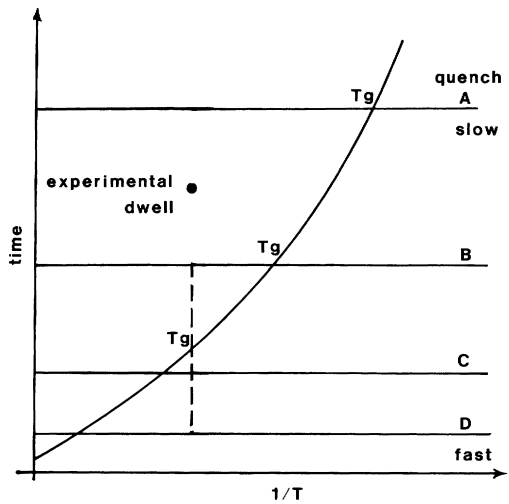

Fig. 8. Illustration of the relationship between quench rate, dwell point and the glass transition in silicate melt studies. Of the four experimental quenches of the sample from the equilibrated dwell point, only the fast quenches, C and D record the speciation extant at the dwell temperature. Quench rates A and B are too slow and the sample re-equilibrates during the quench to a lower glass transition value (T_g). A quench rate-dependence of speciation here indicates a temperature-dependence of speciation in the liquid.

transition temperature. Fig. 8 illustrates four cases that are distinguishable with respect to the dwell point and the τ curve: A, B, C, and D. In case A, a slow quench rate has been chosen. The dwell time of the experiment is shorter than the equilibration timescale corresponding to the quench rate. The equilibration time of the quench intersects the τ curve at a lower temperature than the dwell temperature. This intersection of the q curve with the τ curve is the fictive temperature, the effective temperature of last equilibration of the cooling liquid. In case B, a faster quench rate has been chosen, the timescale corresponding to the chosen quench rate is shorter than the equilibration time of the dwell point and thus the quench or q curve crosses the τ curve at a point that is at lower temperature than the dwell temperature, but *at higher temperature than the fictive temperature of case A.* This last point is crucial. Two different quench rates yield two different equilibration temperatures. Thus knowledge of the location of q and τ curves permits the calculation of equilibration temperatures as a function of quench rate. Continuing with case C, the quench rate has again been increased. In this case the equilibration time corresponding to the

quench rate is high enough that the q curve crosses the τ curve at a temperature above the dwell temperature. The intersection of the q and τ curves no longer defines the glass transition temperature, which is fixed instead at the dwell temperature. Comparison of cases B and C illustrates that it is the lower of the dwell temperature or the τ curve — q curve intersection temperature, that defines the fictive temperature of the resultant glass. In practice, the quench rates needed to achieve case C are quite high, see below. Case C is assumed implicitly (and often incorrectly) in studies that assign dwell temperatures to glass spectra in order to infer high temperature liquid structure, from glass data.

Finally, the fictive temperature obtained in case D is equal to that for case C. The experimental observation of a quench rate-dependence of speciation or properties corresponds to cases equivalent to A and B. An experimental observation of quench rate-independent structure or properties may correspond to cases C and D. If a quench rate-dependence is observed, then (1) the property must be temperature-dependent, (2) the resultant properties cannot correspond to the dwell temperature of the experiment and (3) the true temperature-dependence of the property can be estimated from an analysis of the q and τ curves. If a quench rate-dependence of the measured property is not observed, then either (1) the property is not measurably temperature-dependent, (2) the range of quench rates is too small or the slope of the τ curve is too high to access a sufficient range of fictive temperature or (3) the actual dwell temperature state is being preserved (Fig. 8, case C and D). This discussion is quantified below. We note here that recent studies of silicate glasses have demonstrated a significant quench rate- (and thus temperature-) dependence of speciation for reactions involving Na and H in silicate liquids (Brandriss & Stebbins, 1988; Silver, 1988, respectively).

3.2. Equilibration and preservation

A common experimental strategy for the investigation of silicate melt structure by studying glass properties is to dwell a melt at high temperature for a certain time and then to quench the melt as fast as possible, using a single quench rate.

Three possibilities exist for the dwell equilibration and subsequent re-equilibration during quenching of speciation and properties in silicate

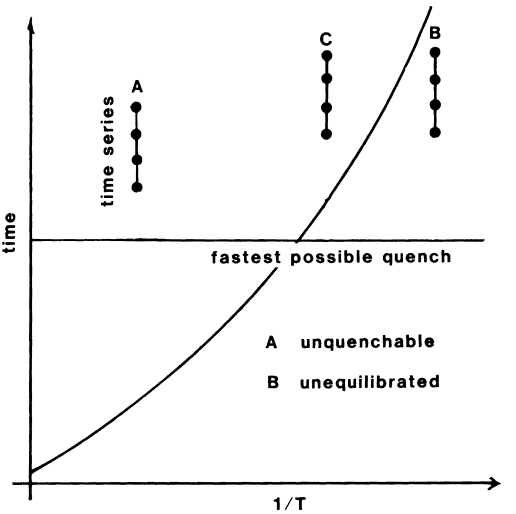

Fig. 9. Equilibration versus preservation in silicate melt studies. Case A is an equilibrated but unquenchable state. Case B is an unequilibrated but quenchable state. Case C is an equilibrated and quenchable state.

liquids that are quenched to glasses. These are schematically illustrated in Fig. 9 where three cases, using the same single quench rate, are illustrated. Cases A, B and C have different relationships to the τ curve. Each case portrays a time series of experiments; the sort of test for equilibration that is often carried out in silicate liquid studies. The experiments of increasing duration are represented by a series of points lying on vertical (isothermal) lines. In case A all the experiments lie well above the relaxation curve (i.e. at longer times and higher temperatures) and the melt is equilibrated (i.e. a relaxed liquid). Upon the fastest possible quench however, case A yields an equilibration temperature (q — τ intersection) that is considerably below the dwell temperature. In other words, case A is equilibrated but unquenchable. Case B is a time series of experiments that have not achieved equilibrium. The location of the dwell points below (at shorter times and lower temperatures than) the τ curve indicate this and also indicate that the speciation obtained during these experiments will be preserved during the quench. These experiments are unequilibrated but quenchable. The evidence of such behavior would be a time-dependence of speciation if the time series approaches the τ curve. (If the time series remains remote from the τ curve, then no change will occur in the starting glass.) Case C is the desired case. In this case the experiments have

equilibrated as indicated by their position with respect to the τ curve and the dwell temperature has been preserved because the quench rate corresponds to an equilibration timescale shorter than the liquid's relaxation time (the τ curve) at this temperature. Clearly, case C is the goal in studies of liquid structure conducted on quench glasses that assign the resultant data to the dwell temperature of the experiment. Case C does not hold for many experiments performed on low viscosity liquids using currently available quenching techniques. The consequence of this is that quench rate must be used as an independent variable in such glass studies.

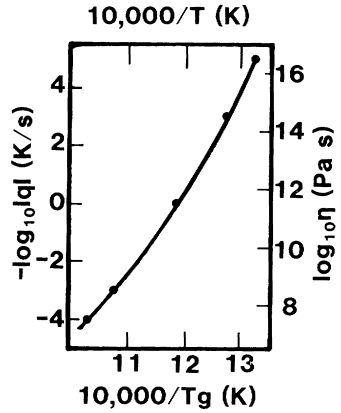

Fig. 10. The quantification of relaxation times corresponding to quench rates. Comparison of the quench rate-dependence of the glass transition using differential scanning calorimetry (dots) with the temperature-dependence of viscosity (line) reveals similar slopes linking enthalpic and shear relaxation at the glass transition. (Redrawn from Scherer, 1984.)

3.3. Quantifying q

The observed quench rate-dependence of speciation and properties of glasses can be used to quantitatively reconstruct the temperature-dependence of the structure and properties of silicate liquids, the goal of many workers (e.g., Seifert *et al.*, 1981; Liu *et al.*, 1988).

As noted above, the simplest model for predicting viscous versus elastic response is that of Maxwell (1867) where the timescale that divides viscous from elastic behavior is given by the ratio of the shear viscosity to the shear modulus (Eqn. (1)). Although equation (1) is not an exact description of relaxation/equilibration in complex silicate melts (Fig. 3) or glasses with complex thermal history, several workers have demonstrated that the location of the mean relaxation time corresponding to the glass transition in temperature-time space may be closely approximated using Eqn. (1) (Moynihan *et al.*, 1976; Scherer, 1986; Narayanaswamy, 1988).

The calculation of q curves is derived from the scan rate-dependence of the glass transition temperature in scanning calorimetry (e.g., Scherer, 1984). When this scan rate — glass transition temperature is compared with the temperature-dependence of viscosity (Fig. 10), equivalent slopes are obtained, as would be expected if the microscopic origin of these shear and enthalpic relaxations is the same. Given an equivalence of mechanical (shear) and enthalpic relaxation in silicate liquids the relaxation time (Eqn. (1)) pertaining to a given scan (quench) rate can be obtained via

$$\log_{10}\eta^*(\text{Pa s}) = \log_{10}10^{11.3}(\text{Pa K}) - \log_{10}|\mathbf{q}|\,(\text{K/s}) = \log_{10}\tau_q(\text{s}) + \log_{10}G_\infty(\text{Pa}) \qquad (5)$$

where q is the quench rate, η^* is the viscosity at the glass transition (Scherer, 1984) and τ_q is the equilibration time of the quench or q curve; this has been done in several glass science studies (DeBolt *et al.*, 1976; Scherer, 1986; Crichton & Moynihan, 1988).

Now that the q and τ curves (see section 2.2) have been quantified they can be plotted in temperature-time space and the fictive temperature of a given class can be read as their intersection. The viscosity for most simple silicate melts can be found in one of the literature reviews (e.g., Bansal & Doremus, 1986; Ryan & Blevins, 1987). Complex melt viscosities can be estimated from the schemes of Bottinga & Weill (1972) or Shaw (1972), usually to an accuracy of $\pm$ 0.5 $\log_{10}$ units. The shear modulus or modulus of rigidity in Eqn. (1) is that for the glass. Bansal & Doremus (1986) have compiled G_∞ values for a wide range of silicate glasses. Their compilation indicates that the composition- and temperature-dependence of G_∞ is very slight (relative to viscosity variations).

The fastest quench rates used in silicate glass work are limited by the thermal conduction within a quenching sample of the required size. Drop quenches are probably no better than $\cong$ 500 °C/s. Faster quench techniques on smaller samples can extend this range to $\cong 10^4$—10^5 °C/sec. The slowest quench rates are limited by phase separation concerns (i.e., crystallization or liquation) and this constraint varies widely with melt composition. Rate cooling as slow as degrees per hour is

probably a generous lower limit on experimental q values. This yields a range of approx. 3.5 $\log_{10}$ units of q accessible for silicate liquids. A quench rate of 500 °C/s yields fictive temperatures of approximately 1500, 1100, 800 and 550 °C for SiO_2, $NaAlSi_3O_8$, $CaMgSi_2O_6$ and $Na_2Si_2O_5$ liquids, respectively. Although the viscosity data are less well constrained, the fictive temperatures (at 500 °C/s) for anhydrous rhyolite, andesite and basalt are, approximately, 1100, 800, and 600 °C, respectively. The assignment of homogeneous equilibria obtained from glass spectra, to temperatures above these limits, presumes that such displacive equilibria can be frozen in well above the glass transition: an assumption that has no experimental support.

We have seen that both viscosity and quench rate are linearly proportional to relaxation time. The relaxation time corresponding to the dwell temperature of an experiment is the relaxation time that must be achieved by the quench to preserve the equilibria. We can quantify this in terms of an inequality corresponding to equation (5).

$$\log_{10}\eta^* \text{ (Pa s)} \geq \log_{10} 10^{11.3} \text{(Pa K)} - \log_{10}|q| \text{ (K/s)} \quad (6).$$

In order to preserve the structure of a melt residing at a dwell temperature, the quench rate must be chosen so that relationship (6) holds for the viscosity of the melt at that temperature. Alternatively, the maximum temperature structure quenchable using a known quench rate is given by the temperature at which the viscosity of the liquid yields an equality for relationship (6).

3.4. Water — an example

The reaction to be considered is

$$2OH^- \leftrightharpoons H_2O + O_m^{2-} \quad (7)$$

where H_2O is molecular water, O_m^{2-} is a "dry" oxygen (structurally bound to an anhydrous component of the melt) and OH^- is a hydroxyl group dissolved in the melt. In a fully polymerized melt such as rhyolite, the dry oxygen is a "bridging oxygen", bonded to two tetrahedral cations, and represents the strongest bonds in the liquid. Thus a bridging bond must be broken for reaction (7) to proceed to the left and one must be formed for progress to the right. In a situation where all reactants are in the vicinity of the reaction site, we can reasonably suppose that the progress of reaction (7) will be rate-limited by the formation and breakage of the strongest bond in the reaction. For the case of reaction (7) this leads to the conclusion that the exchange frequency of the oxygen bridging bonds to O_m^{2-} is the rate-limiting step. This exchange frequency corresponds to the structural relaxation time of rhyolite melt (Webb & Dingwell, 1990a). Thus the τ curves of hydrous rhyolite should record the glass transition with respect to reaction (7).

One further consideration concerns the concentration of reactant OH^- in the melt. Water contents from 1 to 3 wt. % correspond to minimum (undissociated) mole fractions of 0.02 to 0.09. Two to 9 % of the oxygen atoms are therefore coordinated by hydrogens (any dissociation increases this number). Thus (in the most ordered case) the OH^- component could be spaced out by several Si-O bond lengths. In this case, diffusion of a second OH^- to the reaction site is necessary because 2 OH^- are required for reaction (7). It is conceivable that this diffusion could rate-limit reaction (7) when progressing to the right (i.e., during a quench). To evaluate this possibility we can calculate the average spacing of hydrous species (in units of oxygen bond lengths) in a rhyolite melt at a given concentration of dissolved water, as the cube root of the reciprocal of the mole fraction. For 1 wt. % water (2 mole %), the average spacing is the cube root of 1/0.02 which is 3.7. Thus a diffusive lengthscale of hydrous species 3.7 times as large as the oxygen diffusive lengthscale will suffice to provide a second OH^- to the reaction site at the rate of reaction progress defined by the oxygen mobility. This translates into a factor of 13.7 (a $\log_{10}$ factor of 1.2, through $Dt = x^2$) for the relative diffusivities of hydrous species and oxygen. This value is far less than that recorded for the relative tracer or self-diffusivities of hydrous species versus oxygen in SiO_2 (Brückner, 1971). For type II silica (150—400 ppm OH^-), at temperatures of 400—700 °C the diffusivity of OH^- is approximately 10 $\log_{10}$ units higher than that of oxygen, and hydrogen diffusivity is 5 $\log_{10}$ units higher than that of OH^- (Brückner, 1971). This observation leads us to conclude that reaction (7)'s progress to the right during quenching is not rate-limited by the hydrous species mobility; and that the τ curves of hydrous rhyolite do indeed record the glass transition with respect to reaction (7).

Silver's (1988) study of the effect of composition on the speciation of water in silicate glasses includes a set of data illustrating the quench-rate dependence of the proportions of molecular water and water dissolved as hydroxyls in rhyolite melts (Fig. 11). These speciation — quench rate

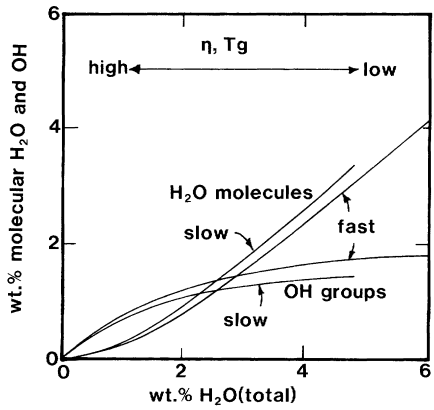

Fig. 11. The quench rate dependence of water speciation illustrated by the data of Silver (1988). Water dissolved in silicate melts dissociates with increasing temperature. A slower quench rate yields more molecular water. This plot cannot be considered an isothermal comparison of water speciation because the glass transition temperature varies with water content. (Redrawn from Silver, 1988.)

data (Table 13, (Silver, 1988)), combined with calculated τ curves for the hydrous rhyolites permit us to estimate the temperature-dependence of the speciation reaction.

In Fig. 12 we have plotted the viscosity-temperature relationships (calculated using the method of Shaw (1972)) for the KS rhyolite of Silver (1988) with 1, 3 and 5 wt. % H_2O added. When transformed using equation (1) these represent τ curves for these compositions. We have also plotted the q curves for the quench rates estimated by Silver (1988) for her rapid quench (200 °C/s) and air quench (200 °C/m) techniques, using equation (5). The fictive temperatures for each glass may be read from Fig. 12 as the intersections of the q and τ curves. In Fig. 13 we have plotted the quench rate — speciation data (interpolated from Table 13 of Silver (1988)) versus the reciprocal of the (fictive) temperature. We present the temperature-dependence of the water speciation data as

$$k = a(H_2O) \cdot a(O_m^{2-})/a(OH^-)^2 \qquad (8)$$

where k is the equilibrium constant of equation (7), and $a(H_2O)$, $a(O_m)$ and $a(OH^-)$ are the activities of molecular water, dry oxygen (in the melt but not associated with any H atoms) and hydroxyl groups dissolved in the melt. If we assume the simplest case of ideal mixing of species in equation (7) then the activities in equation (8) may be replaced by mole fractions. The value of ln k will then vary as a linear function of reciprocal absolute temperature

$$\ln k = -\Delta G/RT \qquad (9)$$

where G is the free energy of the reaction and R is the gas constant. In Fig. 13a, the error estimate for 1/T derives from the uncertainty in calculated viscosity which Shaw (1972) gives as a factor of 2

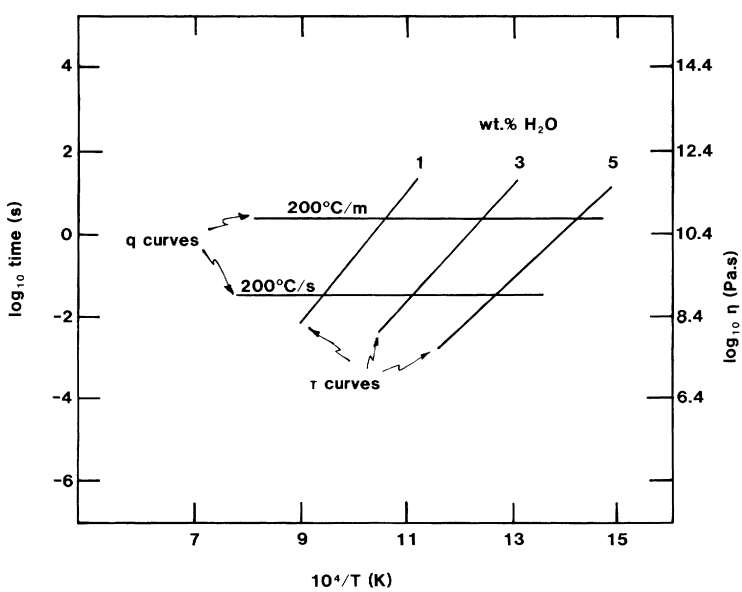

Fig. 12. The derivation of fictive temperatures for the hydrous rhyolites of Silver (1988). The q curves are for quench rates of 200 °C/s and 200 °C/minute, the τ curves are for KS rhyolite with 0, 1, 3, 5 wt. % water. The intersections of q and τ curves yield the fictive temperatures.

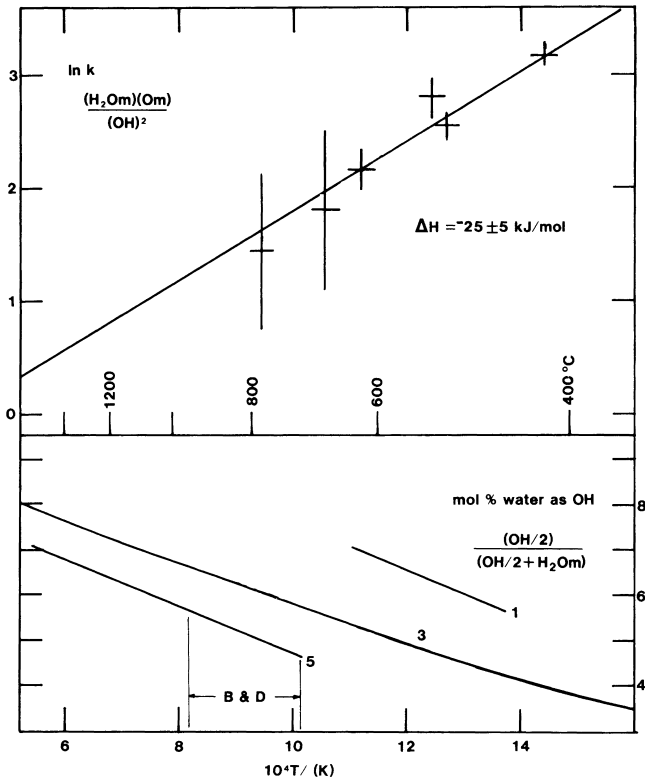

Fig. 13. (a, top) The temperature-dependence of the value of the equilibrium constant of Eqn. (7) expressed as the natural log (i.e. ln k). The extrapolations to higher teperature and water contents are linear in ln k. B & D refers to the region of P-V-T data for "albite"-H_2O (Burnham & Davis, 1971). (b, bottom) The proportions of water dissolved in rhyolite melt as dissociated and molecular species, as a function of temperature. (Calculated using the best fit line of Fig. 13a, for 1, 3 and 5 wt. % water dissolved.)

and the uncertainty in ln k is derived from propagating an analytical (infrared spectroscopy (Silver, 1988)) error of ± 0.1 wt. % H_2O or OH^- through equation (8). It can now be seen (Fig. 13a) that, when the hydrous rhyolite glasses (Silver, 1988) are corrected to their fictive temperatures, the proportion of hydroxyl increases strongly with increasing temperature. At a constant fictive temperature, the proportion of hydroxyl decreases with increasing water content, but the effect is diminished compared to what has previously been proposed (Stolper, 1982a, b).

To clarify this last point, in Fig. 13b we have plotted our estimates (from Fig. 13a) of water dissolved as H_2O and OH^- as a function of temperature. Fig. 13b indicates that dissociated water (OH^-) dominates the speciation of water dissolved in moderately water-rich (up to 3 wt. %) rhyolite melts above 800 °C.

The strong shift of fictive temperature (and thus temperature of last equilibration during the quench) with water content means that comparisons of glasses varying widely in water content but quenched at the same rate cannot be considered isothermal comparisons.

4. Non-Newtonian rheology

4.1. Fiber elongation

The onset of non-Newtonian rheology in silicate melts has been investigated recently by Webb & Dingwell (1990a, b) using fiber elongation techniques. Four melt compositions, chosen to represent a wide chemical range of geological melts, were investigated. The compositions are a high silica rhyolite from Little Class Mountain, an andesite from Crater Lake, a tholeiitic basalt from Hawaii and an "average" nephelinite from the compilation by Chayes (1975; see Mysen, 1987).

In fiber elongation measurements, the viscosity is determined as the ratio of the applied tensile stress to the observed strain rate. In this geometry, the observed viscosity is the elongational viscosity, η_{elong}, and is related to the shear viscosity η_s by;

$$\eta_{elong} = \frac{\sigma}{\dot{\varepsilon}} = \frac{9\,\eta_v \eta_s}{3\,\eta_v + \eta_s} \qquad (10)$$

where η_v is the volume viscosity (e.g. Mazurin, 1986), σ is the stress and $\dot{\varepsilon}$ is the strain rate.

Temperature was chosen to set the viscosity to $\sim 10^{12}$ Pa s and each fiber was initially annealed at temperature for a period of 10^4 s. This equilibration time is greater than both the shear and volume relaxation times of a melt with $\eta_V = \eta_S \approx 10^{12}$ Pa s and G_∞ (shear modulus) $\approx K_\infty$ (bulk modulus) ≈ 10 GPa ($\tau_V = \tau_S = 100$ s). The determinations of non-Newtonian viscosity were begun with an initial stress of 10 MPa ($\dot{\varepsilon} \sim 10^{-5}$); the applied stress being increased stepwise to ~100 MPa until either the fiber broke or the limit of travel of the dilatometer was reached.

Although infinite shear strains are possible in a melt, volume strain must be limited in magnitude (Mazurin, 1986). Volume viscosity therefore approaches an infinite value with increasing time, and Eqn. (10) becomes;

$$\eta_{elong} = 3\,\eta_S \qquad (11)$$

for time $>> \tau$. For periods >100 s, the shear viscosity calculated using Eqn. (11) is at most 0.02 $\log_{10}$ Pa s less than the relaxed shear viscosity.

The critical data illustrating non-Newtonian behavior are illustrated in Fig. 14 and 15. In Fig. 14, high strain rate viscosity data for the rhyolite (LGM), andesite (CLA), basalt (HTB) and nephelinite (NEP) are plotted as functions of strain rate, at temperatures of 818, 754, 716 and 673 °C, respectively. Each melt exhibits similar behavior, with viscosity remaining constant over a range of low strain-rates, decreasing as the strain rate is increased. The log stress versus log strain rate for these melts is plotted in Fig. 15. Departure from Newtonian behavior is illustrated by the deviation from a slope of 1 for strain rates $> 5 \times 10^{-5}$ s^{-1}.

4.2. Maxwell approximation

The temperature at which each melt composition was investigated was chosen in order to set the shear viscosity to $\sim 10^{12}$ Pa s. The relaxation time calculated from Eqn. (1) for this viscosity is 100 s; corresponding to a relaxation strain-rate of $\sim 1 \times 10^{-2}$s^{-1}, where $\dot{\varepsilon}_{relax} = \tau^{-1}$. The calculated relaxation strain rates are plotted, for each composition, as arrows in Fig. 14. The deviation from a Newtonian relationship occurs at strain rates which are ~3 orders of magnitude less than the calculated relaxation strain rates. In the case of melts described by a single relaxation time, a 2% deviation from relaxed behavior is expected to occur 2 orders of magnitude below the relaxation strain rate. A number of studies of silicate melts in the

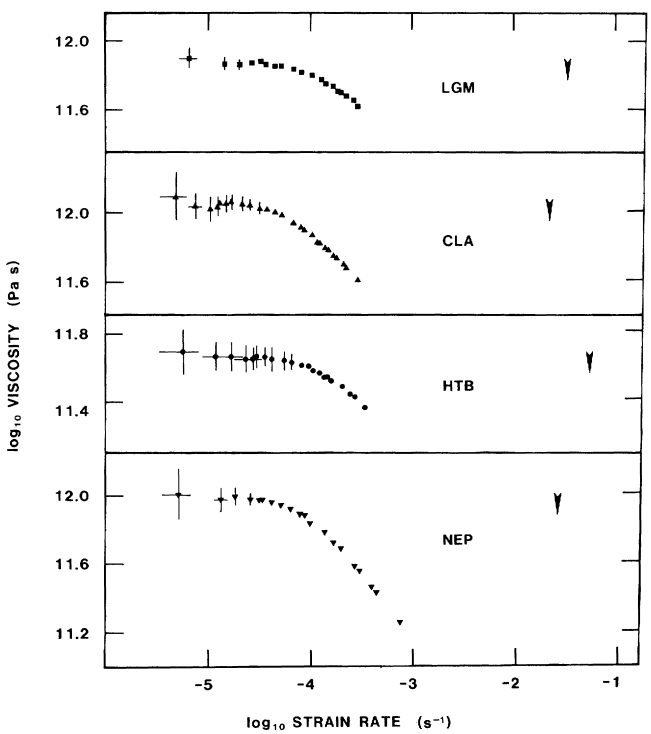

Fig. 14. Shear viscosity of Little Glass Mountain rhyolite, Crater Lake andesite, Hawaiian tholeiite, and nephelinite as functions of strain rate. The arrows indicate the calculated relaxation strain rates. (Redrawn from Webb & Dingwell, 1990a.)

glass transition region (e.g., torsional, Mills, 1974; ultrasonics, Sato & Manghnani, 1985), however, indicate more complex relaxation behavior than that described by a single relaxation time. Any distribution of shear relaxation times results in a broadening of the width of the relaxation zone and the occurrence of non-relaxed behavior at lower strain rates than predicted from single relaxation strain rate theory. This onset of non-Newtonian shear viscosity is a consequence of the rate of shear deformation approaching the rate of Si-O bond exchange.

4.3. Time versus frequency domain

These fiber elongation studies underline an important distinction to be made between low strain measurements of the glass transition (i.e. frequency domain studies such as mechanical torsion or ultrasonic wave propagation experiments) and high strain measurements such as fiber elongation. Both types of experiments observe non-Newtonian viscosity as a frequency- or strain rate-dependence of the stress — strain rate ratio. In frequency domain experiments, the frequency of the applied stress may be increased through the glass transition frequency ($\tau^{-1} = 2\pi f$) and the shape of the relaxation function recorded. In time domain experiments, however, the stress required to reach strain rates approaching the relaxation strain rate, $\dot{\varepsilon}_{relax}$, approximates the tensile strength of the melt, and the material fails before $\dot{\varepsilon}_{relax}$ is reached. Fig. 16 is a plot of the location of the propagation of longitudinal shock (Rigden *et al.*, 1988) and ultrasonic (Sato & Manghnani, 1985) waves in rhyolitic melts in time-temperature space. The fiber elongation location is from Webb & Dingwell (1990a). The relaxation or τ curve of the LGM rhyolite is plotted using the viscosity data of Webb & Dingwell (1990a) at low temperatures, and the method of Shaw (1972) at higher temperatures in combination with the Maxwell relation.

The strain rate — temperature range of two time-domain methods that have been used with rhyolite melts are also plotted in Fig. 16; the con-

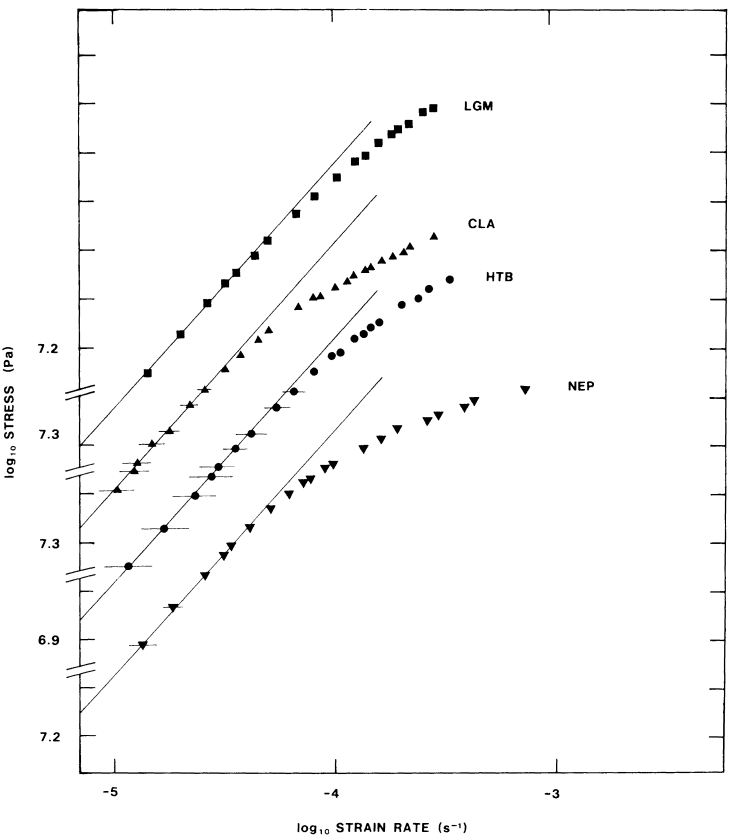

Fig. 15. Stress versus strain rate for Little Glass Mountain rhyolite, Crater Lake andesite, Hawaiian tholeiite, and nephelinite. Vertical scale is 0.2 $\log_{10}$ Pa s. Lines of slope = 1 — representing a linear stress — strain rate relationship — are fit to each set of data. (Redrawn from Webb & Dingwell, 1990a.)

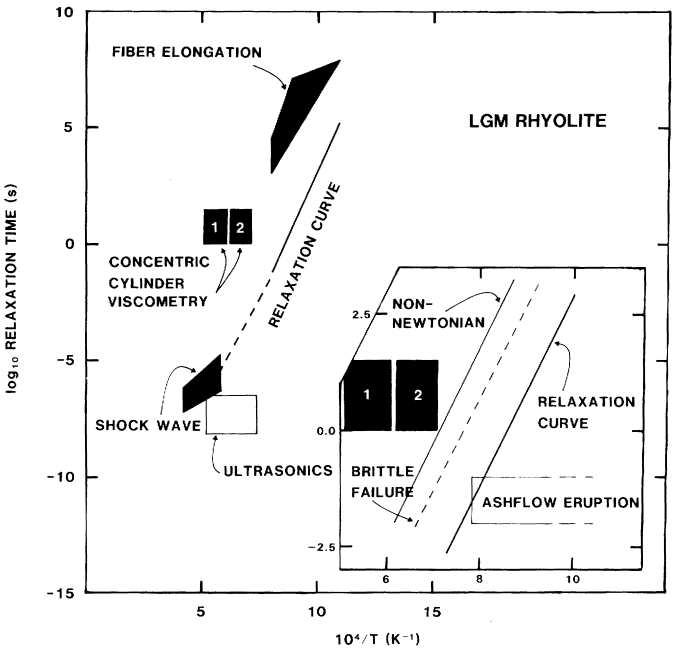

Fig. 16. Locations of various experimental techniques with respect to structural relaxation in Little Glass Mountain rhyolite. The relaxation curve is calculated from the measurements of Webb & Dingwell (1990a) (solid line) and from the method of Shaw (1972) (dashed line). The concentric-cylinder viscometry methods are (1) normal torque (Dingwell *et al.*, 1985) and (2) high torque (Spera *et al.*, 1988). The shock wave location is calculated from Rigden *et al.* (1988). The ultrasonics location is that of Sato & Manghnani (1985). (Redrawn from Webb & Dingwell, 1990a.)

centric cylinder (Dingwell *et al.*, 1985; Spera *et al.*, 1988) and fiber elongation (Webb & Dingwell, 1990a, b) methods. The study of Webb & Dingwell (1990a) illustrates that, as in frequency-domain experiments, the fiber elongation technique records the onset of non-Newtonian behavior in the melt. However, it is possible that the large non-equilibrium strains associated with this technique result in structural anisotropy of the melt (Brückner, 1987). If these structural changes are significant with respect to viscous flow, the two types of measurements — low strain, frequency domain and high strain, time domain — may not necessarily result in equivalent non-equilibrium properties being observed in the non-Newtonian region.

4.4. Brittle failure

The ultimate result of loading the melt fibers to the high stresses required to reach non-Newtonian strain rates is brittle failure of the fiber. Such failure is observed to occur without tapering or necking of the fiber. This observation of brittle failure illustrates that in natural processes, stresses high enough to induce brittle failure are also capable of inducing non-Newtonian flow. Observation of this relationship between high stresses, brittle failure and non-Newtonian flow would not be possible from investigations of the glass transition made using frequency domain techniques alone.

The inset of Fig. 16 illustrates the relationship beween the onset of non-Newtonian flow, the brittle failure of the fiber and the τ curve, calculated from the Maxwell relationship. The three phenomena are, to a first approximation, parallel curves in strain rate — temperature space. The non-Newtonian onset occurs three log units of time above the relaxation curve. This is followed, in the case of continued flow at increasing strain rate, by the brittle failure curve, ~2 $\log_{10}$ units above the relaxation curve; as observed by Simmons *et al.* (1982). This generalization of parallel slopes for the three phenomena is based on the composition- (nephelinite to rhyolite) and temperature-invariance (818—674 °C) of the 3 log unit difference between the non-Newtonian onset and the τ curve (Webb & Dingwell, 1990a, b). This is equivalent to an assumption of thermorheological simplicity (or the time-temperature equivalence principle). While the assumption of thermorheological simplicity works well over the 100—200 degree range of many studies it is possible that more complex behavior would be observed over larger temperature ranges.

4.5. Rhyolitic behavior

Eruptive processes involving rhyolite in this strain rate — temperature range should exhibit such

non-Newtonian stress — strain rate behavior. It is clear from the observation of volcanic ash that brittle failure of the rhyolite occurs during ash flow eruptions. This, combined with Fig. 16 led Webb & Dingwell (1990a) to suggest that the viscous flow of silicate melts during eruptions involving brittle failure of the magma, will pass through a stage of unrelaxed, non-Newtonian deformation. Modeling of the fluid mechanics of magmatic eruptions and of the strain history of rhyolitic glasses should include the consideration of non-Newtonian melt viscosity in the appropriate range of strain rates.

The data of Simmons *et al.*, (1988), Manns & Brückner (1988) and Webb & Dingwell (1990a, b) demonstrate that the occurrence of non-Newtonian viscosity is scaled to the low strain rate, relaxed, Newtonian shear viscosity of the liquid. Although this simplifies the composition-dependence of relaxation in silicate melts, it does not remove it. An isothermal comparison of the Newtonian viscosities of rhyolite and nephelinite melts (a difference of ~4 $\log_{10}$ Pa s at 1400 °C) reveals how sensitive viscosity is to melt composition. After temperature, the most important factor in determining melt viscosity is water content. Qualitatively, the effect of water is to reduce the relaxed melt viscosity and therefore the relaxation time of the melt. During ascent of a crystal-poor, water-bearing rhyolite, it is possible that water loss could increase the relaxation time of the melt into the range of the timescale (strain rate^{-1}) of the magma ascent. If the strain rate were maintained the result would be non-Newtonian flow of the liquid.

The glass transition frequency ($f^{-1} = 2\pi\tau$) also has implications for seismic studies. Taking the onset of non-Newtonian behavior to occur 3 orders of magnitude above the relaxation time; non-linear stress — strain rate behavior and increasing velocity and attenuation of seismic waves is expected to occur for wave-fequencies <10 Hz for melts with shear viscosities $>10^{5.6}$ Pa s (e.g. dry rhyolite at 1050—1250 °C; rhyolite + 5% H_2O at 575—725 °C).

5. Fast relaxations — cationic diffusion

5.1. A relaxation map

The diffusion of certain components of silicate melts can be detached from the timescale of structural relaxation. Tracer diffusivity data indicate that alkali diffusion can proceed much more rapidly than network oxygen and silicon diffusion (e.g., Johnson *et al.*, 1951). The alkali mobility is "decoupled" (Angell, 1988) from the silicate matrix and the temperature dependence of alkali diffusion describes a curve, separate from the structural relaxation curve. This "fast" relaxation curve, corresponding to the timescale of the alkali diffusive jump, is a relaxation timescale for electrical conductivity in silicate melts (e.g., Provenzano *et al.*, 1972).

Fig. 17 is a summary of experimental data concerning structural and fast relaxation in Na_2O-$3SiO_2$ melt. The structural relaxation or glass transition curve is located using the shear viscosity data of Poole (1948) and Bockris *et al.* (1955) and the shear modulus data of Mills (1974) using the Maxwell relation (Eqn. (1)); and by the torsional relaxation study of Mills (1974). The fast relaxation is fixed by the electrical relaxation data of Provenzano *et al.* (1972), by the internal friction (torsional) study of Day & Steinkamp (1971), by the Na tracer diffusivity study of Johnson *et al.* (1951), using

$$Dt = x^2, \tag{12}$$

where x is the Na — Na spacing, t is time and D is the diffusion coefficient and by the electrical conductivity studies of Babcock (1934) and Seddon *et al.* (1932), using Eqn. (4) and the Nernst-Einstein equation,

$$D/\sigma = kT/Ne^2, \tag{13}$$

where σ is the conductivity, k is Boltzmann's constant, T is absolute temperature, N is Avogadro's number and e is the atomic charge (e.g., Havens Verkerk, 1965).

The distribution of the imaginary modulus of the structural and the fast relaxations are illustrated by insets a and b (Fig. 17) of the loss moduli from torsional (Mills, 1974) and electrical (Provenzano *et al.*, 1972) studies, respectively. These loss moduli may result, in detail, from a distribution of relaxation times about the mean values that determine the relaxation lines of Fig. 17. The width of these relaxation functions indicates that the detectable distribution of relaxation behavior about the mean is broad (at least $\pm$ 2 $\log_{10}$ units).

The temperature-dependence of the structural relaxation time forms a non-Arrhenian curve. At an experimental timescale of 10^3 sec it yields a "glass transition temperature" (e.g. calorimetric data of Richet & Bottinga, 1984) of 724 °C.

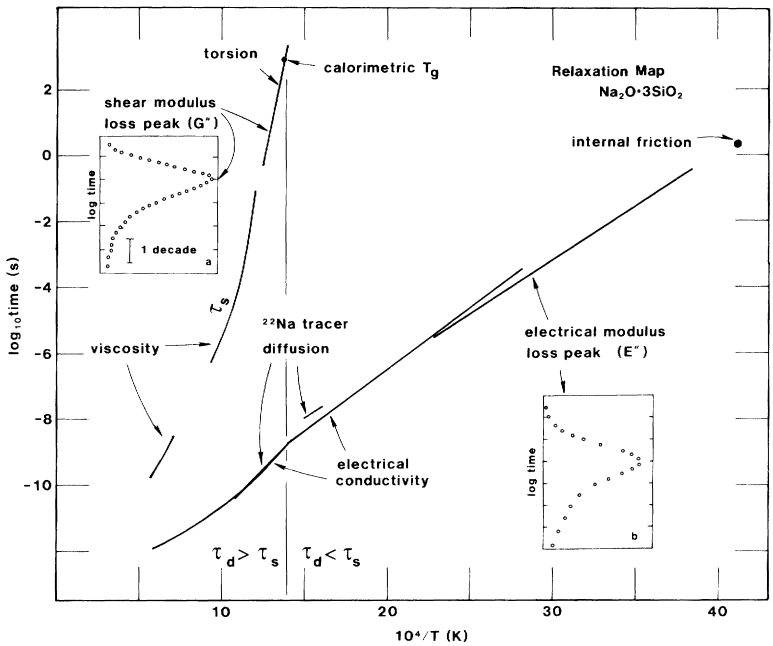

Fig. 17. Relaxation timescales in Na_2O-$3SiO_2$ melt. The inflection in electrical and diffusion data at T_g result from the experimental duration (τ_d) approaching the structural relaxation timescale (τ_s). Structural relaxation data from the torsional study of Mills (1974) and the viscosity studies of Poole (1948) and Bockris *et al.* (1955). Alkali and electrical relaxation data from the tracer diffusion work of Johnson *et al.* (1951), the electrical modulus data of Provenzano *et al.* (1972), the conductivity studies of Babcock (1934) and Seddon *et al.* (1932) and the internal friction data of Day & Steinkamp (1971). T_g calorimetric data from Richet & Bottinga (1984). (Redrawn from Dingwell, 1990.)

5.2. Experimental timescale

Experiments performed with durations (τ_d) shorter than the structural relaxation time (τ_s) will observe a glass whose volume is unrelaxed (τ_d less than τ_s). The only expansivity mechanisms accessible at temperatures below this curve are the elastic, vibrational components. When the combination of duration and temperature of an experiment crosses to the left side of the structural relaxation curve then the volume will relax, using configurational as well as vibrational modes and any volume- or configuration-dependent property measured across this curve should yield an inflection in its temperature-dependence.

The temperature-dependencies of alkali diffusion and of electrical conductivity in Na_2O-$3SiO_2$ melt consist of two segments. The lower temperature electrical conductivity segment is Arrhenian and the upper temperature segment is non-Arrhenian. The two curves intersect where the duration of the experiment (τ_d) equals the structural relaxation time (τ_s) for the temperature of the experiment. In Fig. 17 the location of this inflection is illustrated using comparison of the electrical conductivity studies of Babcock (1934) and Seddon *et al.* (1932) and the Na diffusivity data of Johnson *et al.* (1951). The extrapolation of either segment across the inflection will yield incorrect results. Similar inflections have been noted previously in both synthetic and natural melts (e.g., Dyment *et al.*, 1987; Braedt & Frischat, 1988). The inflection can be expected to be largest in melts that exhibit strong T_g signals in dilatometry and calorimetry and less strong in glasses such as SiO_2 that exhibit weak T_g signals. Thus, diffusivity data obtained on unrelaxed glasses are not directly comparable with data obtained on relaxed liquids. We emphasize that the temperature of this inflection only corresponds to the calorimetric glass transition temperature because the timescales of the two experiments are similar. Experiments performed on longer timescales will exhibit a lower temperature inflection because the samples will relax at lower temperatures.

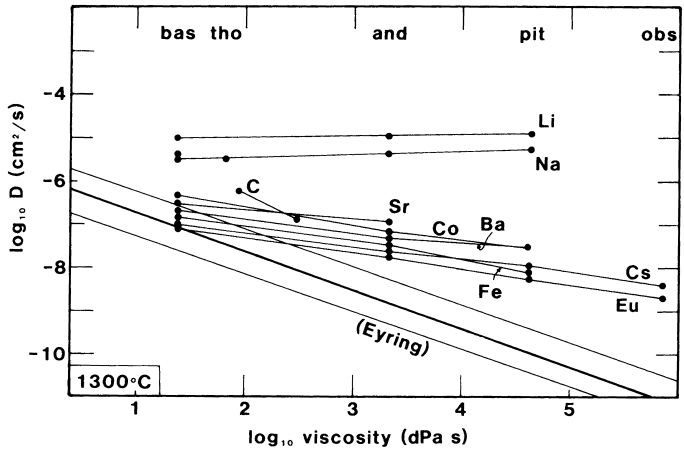

Fig. 18. Cationic tracer diffusivity data (Watson *et al.*, 1982; Henderson *et al.*, 1985) versus melt viscosity (calculated using the method of Shaw (1972)). The diffusivity of oxygen is calculated from the Eyring relation. All data at 1300 °C. Note that the diffusivities of Sr, Co, Ba, Fe, Cs, Eu and C cluster near the calculated oxygen diffusivity. (Redrawn from Dingwell, 1990.)

5.3. Observation timescale

A further consequence of relaxation in silicate melts concerns the timescale of cationic diffusion relative to network O and Si diffusion. In a diffusion experiment the jump frequency of the diffusing tracer cation corresponds to a timescale that can be considered the characteristic or observational timescale of the experimental probe (τ_p). In silicate melts all cations are bonded to network oxygens. The network oxygen diffusivity is controlled by the exchange frequency of oxygen anions. During such exchanges the bonds to cations are temporarily broken and the cation is free to diffuse. At relatively low oxygen mobilities (e.g., high viscosities) the diffusivities of some cations are so much faster than oxygen that the network oxygens appear in fixed structural sites during a diffusive jump. At higher temperatures the cationic and oxygen diffusivities converge until the cationic diffusivities are only 1—2 $\log_{10}$ units faster than the network oxyen and silicon diffusivities obtained from the Eyring equation. At this point Si-O exchanges are occurring at 1 to 10% of the frequency of cation jumps and should influence the cationic diffusivities.

Henderson *et al.* (1985) have reported tracer diffusivity data for Li, Na, Ba, Co, Sr, Fe, Cs and Eu in basalt, andesite, pantellerite, pitchstone and rhyolite melts. They have observed two types of composition-dependence of diffusivity. Li and Na exhibit a slight increase in diffusivity whereas Ba, Co, Fe, Cs, Sr and Eu exhibit a strong decrease in diffusivity with increasing SiO_2 content. The Na and Li data may be explained using the concept of anionic porosity (Dowty, 1980) with increasing silica content from basalt to rhyolite decreasing the volume fraction of the melt occupied by oxygen anions. The increase in free volume or porosity could permit higher diffusivities for cations.

The Sr, Ba, Fe, Cs, and Eu data of Henderson *et al.* (1985) cannot be explained using the anionic porosity concept. The slower cations (Ba, Co, Sr, Fe, Cs, Eu) differ strongly in ionic radii and charge but exhibit similar diffusivity behavior. The 1300 °C diffusivity data of Henderson *et al.* (1985) are plotted in Fig. 18 as a function of melt viscosity. The melt viscosities were calculated using the method of Shaw (1972, $\pm$ 0.5 $\log_{10}$ units). The network O and Si diffusivities, derived from the Eyring equation, are presented as a solid line in Fig. 18. Also in Fig. 18 are C tracer diffusion data of Watson *et al.* (1982) for synthetic Na_2O-Al_2O_3-SiO_2 and basaltic melts. The C data coincide with the slower group of Henderson *et al.* (1985). The Eyring diffusivity approaches that of Ba, Co, Sr and Cs with decreasing viscosity. The maximum separation, at obsidian, is less than 2 $\log_{10}$ units indicating that the mean jump frequency of network oxygen and silicon is more than 1% of the cationic jump frequencies. It is important to point out that the diffusivity data represent mean mobilities. The range of mobilities are emphasized in the loss moduli insets a and b of Fig. 17. As noted above, the detectable widths of the shear (oxygen diffusion) and electrical (Na diffusion) relaxation timescales are approximately $\pm$ 2 $\log_{10}$ units. Thus, it has been proposed (Dingwell, 1990) that the compositional dependence of the Co, Sr, Ba, Eu, Fe and C diffusivities at 1300 °C (Fig. 19) results from their proximity (less than 2 $\log_{10}$ units) to the Eyring diffusivity.

The oxygen and cationic diffusivities diverge at higher viscosities (Fig. 19) and are positive func-

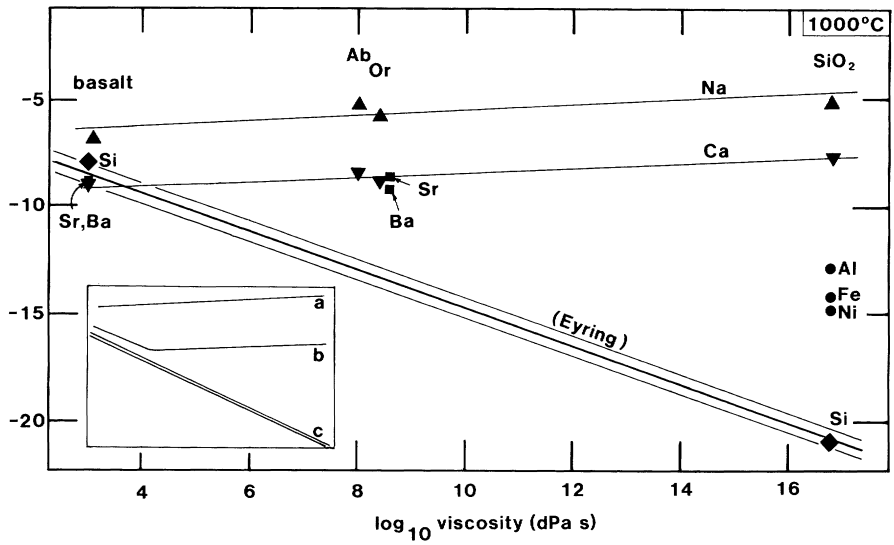

Fig. 19. Tracer diffusivity data versus melt viscosity for basalt, a Ca-Al-Si synthetic oxide melt, albite and orthoclase melts, and SiO_2 melt at 1000 °C. Note that the composition-dependence of Ca diffusivity is a slight positive dependence on SiO_2 content, apparently unrelated to viscosity/oxygen diffusivity. Data sources: Atkinson & Gardner, 1980; Brebec *et al.*, 1980; Frischat, 1969; Frischat, 1975; Ghoshtagore, 1969; Hofmann & Magaritz, 1977; Jambon, 1982; Jambon & Carron, 1976; Jambon & Carron, 1978; Magaritz & Hofmann, 1978. (Redrawn from Dingwell, 1990.) Vertical scale same as in Fig. 18.

tions of silica content. The Ca, Sr and Ba diffusivity data in Fig. 19 exhibit a composition dependence similar to that of Na, in contrast to the composition-dependence of Ba and Sr diffusion at 1300 °C (Fig. 18). It appears that, at 1000 °C, the Ca, Sr and Ba diffusivities are too far removed from network oxygen mobility to be affected by it. The compositional-dependence of Ca, Ba and Sr in a static oxide matrix is being observed.

Also illustrated in Fig. 19 are diffusivity data for Al, Fe, Ni and Si in SiO_2 glass and for Si in a CaO-Al_2O_3-SiO_2 melt. The diffusivities of Al, Fe and Ni in SiO_2 are well removed from the Eyring diffusivity and thus they are predicted to have decreasing diffusivity with decreasing silica content, until their diffusivity approaches the Eyring curve. The diffusivity of Si lies on the Eyring oxygen diffusivity curve both for SiO_2 and for the Ca-Al-Si melt, (at viscosities 14 orders of magnitude in difference). These data appear to indicate that Si diffusivity is controlled by the exchange frequency of Si-O bonds. The case for oxygen diffusion is complicated by the presence of physically dissolved oxygen in the melts which participates in bulk oxygen diffusion at relatively high O_2 pressures (Williams, 1965; Schaeffer, 1984).

The inset of Fig. 19 illustrates the three possible cases of composition dependence expected from the above discussion. In case a, the slight positive dependence of diffusivity of silica content is unrelated to viscosity (e.g. Na and Li in Fig. 18 and 19). In case c the cationic diffusivity follows the Eyring line (e.g. Si in Fig. 19). The intermediate case b, detached cationic diffusivity at high viscosity and oxygen-related diffusivity at low viscosity, is the behavior observed for Ba and Sr and expected for Al, Fe, Ni, Eu, Co and possibly C.

Finally, self diffusion can also be approximated in binary interdiffusion experiments where the compositional difference between the diffusion endmembers is small. Baker & Watson (1988) have reported that the diffusivity of Al, Fe, Si, Mn, Zn, Y, Zr, and Nb are all within an order of magnitude at 900 to 1400 °C in the rhyolitic melts of their study. Calculated Eyring oxygen diffusivities for their melts are within a log unit of these cationic values. Thus it is proposed that the tight clustering of cationic diffusivities observed in that study result from the convergence to the Eyring diffusivity.

6. Conclusion

The consideration of structural and fast relaxations in silicate melts has opened a new chapter in

our understanding of the dynamics of silicate liquids. Structural relaxation is the origin of the glass transition. Fast relaxations are detached from structural relaxation yielding secondary relaxations at lower temperatures. The atomistic origin of relaxations in silicate melts are now more clearly understood. The variation of melt properties across the timescales of various relaxation processes are of significance for both experimental investigations of melt properties and modeling of igneous magmas during petrogenesis. The relationship between speciation data derived from glasses and the temperature-dependence of liquid speciation and properties can be estimated using quench rate-dependent speciation data and relaxation theory.

Acknowledgements: This paper was presented as a Hauptvortrag at the annual meeting of the Deutsche Mineralogische Gesellschaft in Berlin, September, 1989. Klaus Langer is thanked for the invitation. The original manuscript was significantly improved by the review of Matthias Rosenhauer. We are grateful for discussions of several of the above topics with Austen Angell, Mike Carroll, Charles Ross II, Fritz Seifert and Dave Virgo.

References

Angell, C. A. (1984): Strong and fragile liquids. *In* Ngai, K. L. & Wright, G. B. (eds.), Relaxations in Complex Systems. Office of Naval Research and National Technical Information Service, pp. 3—11.

— (1988): Structural instability and relaxation in liquid and glassy phases near the fragile liquid limit. *J. Non-Cryst. Sol.*, **102,** 205—221.

Angell, C. A. & Torell, L. M. (1983): Short time structural relaxation processes in liquids: comparison of experimental and computer simulation glass transition on picosecond timescales. *J. Chem. Phys.*, **78,** 937—945.

Astin, A. V. (1962): Certificate of viscosity values. Standard sample No. 710 Soda-Lime-Silica Glass. US Dept. of Commerce, Natl. Bur. Stds., Washington DC.

Atkinson, A. & Gardner, J. W. (1980): AERE R-9684. Not seen, quoted from Freer, R. (1981): Diffusion in silicate minerals and glasses: A data digest and guide to the literature. *Contrib. Mineral. Petrol,* **76,** 440—454.

Babcock, C. L. (1934): Viscosity and electrical conductivity of molten glasses. *J. Amer. Cer. Soc.*, 329—342.

Baker, D. R. & Watson, E. B. (1988): Diffusion of major and trace elements in compositionally complex Cl- and F-bearing silicate melts. *J. Non-Cryst. Sol.,* **102,** 62—70.

Bansal, N. P. & Doremus, R. H. (1986): Handbook of Glass Properties. Academic Press, New York, London, pp. 680.

Birge, N. (1986): Specific heat spectroscopy of glycerol and propylene glycol near the glass transition. *Phys. Rev. B,* **34,** 1631—1642.

Bockris, J. O'M., MacKenzie, J. D., Kitchener, J. A. (1955): Viscous flow in silica and binary liquid silicates. *Trans. Farad. Soc.,* **51,** 1734—1748.

Bottinga, Y. & Weill, D. F. (1972): The viscosity of magmatic silicate liquids: a model for calculation. *Amer. J. Sci.,* **72,** 438—475.

Braedt, M. & Frischat, G. H. (1988): Sodium self diffusion in glasses and melts of the system Na_2O-Rb_2O-SiO_2. *Phys. Chem. Glass,* **29,** 214—218.

Brandriss, M. E. & Stebbins, J. F. (1988): Effects of temperature on the structure of silicate liquids: ^{29}Si NMR results. *Geochim. Cosmochim. Acta,* **52,** 2659—2669.

Brebec, G., Seguin, R., Sella, C., Bevenot, J., Martin, J. C. (1980): Diffusion du silicium dans le silice amorphe. *Acta Metall.,* **28,** 327—333.

Brückner, R. (1971): Properties and structure of vitreous silica. II. *J. Non-Cryst. Sol.,* **5,** 177—216.

— (1987): Structural aspects of highly deformed melts. *J. Non-Cryst. Sol.,* **95—96,** 961—968.

Bucaro, J. A. & Dardy, H. D. (1974): High-temperature Brillouin scattering in fused quartz. *J. Appl. Phys.,* **45,** 5324—5329.

Burnham, C. W. & Davis, N. F. (1971): The role of H_2O in silicate melts I. PVT relations in the system $NaAlSi_3O_8$-H_2O to 10 kilobars and 1000 °C. *Amer. J. Sci.,* **270,** 54—79.

Chayes, F. (1975): A world data base for igneous petrology. *Car. Inst. Wash. Yb.,* **74,** 549—500.

Crichton, S. N. & Moynihan, C. T. (1988): Structural relaxation of lead silicate glass. *J. Non-Cryst. Sol.,* **102,** 222—227.

Day, D. E. & Steinkamp, W. E. (1971): *In:* Porai-Koshits, E. A. (ed.), Stekloobraznoye Sostoyaniye, 294—298, Leningrad.

DeBolt, M. A., Easteal, A. J., Macedo, P. B., Moynihan, C. T. (1976): Analysis of structural relaxation in glass using rate heating data. *J. Amer. Cer. Soc.,* **59,** 16—21.

Dingwell, D. B. (1990): Effects of structural relaxation on cationic tracer diffusion in silicate melts. (in press — *Chem. Geol.*)

Dingwell, D. B., Scarfe, C. M., Cronin, D. (1985): The effect of fluorine on viscosities in the system Na_2O-Al_2O_3-SiO_2: implications for phonolites, trachytes and rhyolites. *Amer. Mineral.,* **70,** 80—87.

Dingwell, D. B. & Webb, S. L. (1989a): Structural relaxation in silicate melts and non-Newtonian melt rheology in geologic processes. *Phys. Chem. Minerals.,* **16,** 508—516.

— — (1989b): The temperature dependence of water speciation in rhyolite melts: analysis of quench rate-dependent speciation using relaxation theory. *EOS,* **70,** 501—502 (abstr.).

Dowty, E. (1980): Crystal-chemical factors affecting the mobility of ions in minerals. *Amer. Mineral.,* **65,** 174—182.

Dunn, T. (1982): Oxygen diffusion in three silicate melts along the join diopside-anorthite. *Geochim. Cosmochim. Acta,* **46,** 2293—2299.

Dyment, F., Matzke, Hj., Toscano, E. (1987): Diffusion of ^{83}Rb and ^{84}Rb tracers in waste glasses. *J. Non-Cryst. Sol.*, **93**, 22—34.

Farnan, I. & Stebbins, J. F. (1990): A high temperature ^{29}Si investigation of solid and molten silicates. *J. Amer. Chem. Soc.*, **112**, 32—39.

Frischat, G. H. (1969): Evidence for calcium and aluminum diffusion in SiO_2 glass. *J. Amer. Cer. Soc.*, **52**, 625.

— (1975): Ionic Diffusion in Oxide Glasses, Diffusion Monograph Series. Trans Tech Publications, Aedermannsdorf.

Ghoshtagore, R. N. (1969): Diffusion of nickel in amorphous silicon dioxide and silicon nitride films. *J. Appl. Phys.*, **40**, 4374—4376.

Glasstone, S., Laidler, K. J., Eyring, H. (1941): The theory of rate processes. McGraw-Hill, New York, 611 pp.

Haven, Y. & Verkerk, B. (1965): Diffusion and electrical conductivity of sodium ions in sodium silicate glasses. *Phys. Chem. Glass*, **6**, 38—45.

Henderson, P., Nolan, J., Cunningham, G. C., Lowry, R. K. (1985): Structural controls and mechanisms of diffusion in natural silicate melts. *Contrib. Mineral. Petrol.*, **89**, 263—272.

Hofmaier, G. & Urbain, G. (1968): The viscosity of pure silica. *Sci. Ceram.*, **4**, 25—32.

Hofmann, A. W. & Magaritz, M. (1977): Diffusion of Ca, Sr, Ba and Co in a basaltic melt: implications for the geochemistry of the mantle. *J. Geophys. Res.*, **82**, 5432—5440.

Jambon, A. (1982): Tracer diffusion in granitic melts: experimental results for Na, K, Rb, Cs, Ca, Sr, Ba, Ce, Eu to 1300 °C and a model for calculation. *J. Geophys. Res.*, **87**, 10797—10810.

Jambon, A. & Carron, J. P. (1976): Diffusion of Na, K, Rb and Cs in glasses of albite and orthoclase composition. *Geochim. Cosmochim. Acta*, **40**, 897—903.

— — (1978): Etude expérimentale de la diffusion cationique dans un verre basaltique: alcalins et alcalino-terreux. *Bull. Mineral.*, **101**, 22—26.

Johnson, J. R., Bristow, R. H., Blau, H. H. (1951): Diffusion of ions in some simple glasses. *J. Amer. Cer. Soc.*, **34**, 165—172.

Kampfman, W. & Berckhemer, H. (1985): High temperature experiments on the elastic and anelastic behavior of magmatic rocks. *Phys. Earth Planet. Int.*, **40**, 223—247.

Kurkjian, C. R. (1963): Relaxation of torsional stress in the transformation range of a soda-lime-silica glass. *Phys. Chem. Glass*, **4**, 128—136.

Liu, S-B., Stebbins, J. F., Schneider, E., Pines, A. (1988): Diffusive motion in alkali silicate melts: an NMR study at high temperature. *Geochim. Cosmochim. Acta*, **52**, 527—538.

Magaritz, M. & Hofmann, A. W. (1978): Diffusion of Sr, Ba and Na in obsidian. *Geochim. Cosmochim. Acta*, **42**, 595—605.

Manns, P. & Brückner, R. (1988): Non-Newtonian flow behaviour of soda-lime silicate glass at high deformation rates. *Glastech. Ber.*, **61**, 46—56.

Martens, R. M., Rosenhauer, M., Büttner, H., von Gehlen, K. (1987): Heat capacity and kinetic parameters in the glass transformation interval of diopside, anorthite and albite glass. *Chem. Geol.*, **62**, 49—70.

Maxwell, J. C. (1867): On the dynamical theory of gases. *Phil. Trans. Roy. Soc.*, **A157**, 49—88.

Mazurin, O. V. (1986): Glass relaxation. *J. Non-Cryst. Sol.*, **87**, 392—407.

Mills, J. J. (1974): Low frequency storage and loss moduli of soda silica glasses in the transformation range. *J. Non-Cryst. Sol.*, **14**, 255—268.

Moynihan, C. T., Easteal, A. J., DeBolt, M. A., Tucker, J. (1976): Dependence of the fictive temperature of glass on cooling rate. *J. Amer. Cer. Soc.*, **59**, 12—16.

Muehlenbachs, K. & Schaeffer, H. A. (1977): Oxygen diffusion in vitreous silica — utilization of natural isotopic abundances. *Can. Mineral.*, **15**, 179—184.

Mysen, B. O. (1987): Magmatic silicate melts: relations between bulk composition, structure and properties. *In:* Mysen, B. O. (ed.), Magmatic Processes: Physicochemical Principles. The Geochemical Soc. Spec. Publ. No. 1, 1987.

Narayanaswamy, O. S. (1971): A model of structural relaxation in glass. *J. Amer. Cer. Soc.*, **54**, 491—498.

— (1988): Thermorheological simplicity in the glass transition. *J. Amer. Cer. Soc.*, **71**, 900—904.

Poole, J. P. (1948): Viscosité à basse température des verres alcalino-silicatés. *Verres Refract.*, **2**, 222—228.

Provenzano, V., Boesch, L. P., Volterra, V., Moynihan, C. T., Macedo, P. B. (1972): Electrical relaxation in Na_2O-$3SiO_2$ glass. *J. Amer. Cer. Soc.*, **55**, 492—496.

Richet, P. (1984): Viscosity and configurational entropy of silicate melts. *Geochim. Cosmochim. Acta*, **48**, 471—483.

Richet, P. & Bottinga, Y. (1984): Anorthite, andesine, wollastonite, diopside, cordierite and pyrope: thermodynamics of melting, glass transitions, and properties of the amorphous phases. *Earth Planet. Sci. Lett.*, **67**, 415—432.

Rigden, S. M., Ahrens, T. J., Stolper, E. M. (1988): Shock compression of molen silicate: results for a model basaltic composition: *J. Geophys. Res.*, **93**, 367—382.

Ritland, H. N. (1954): Density phenomena in the transformation range of a borosilicate crown glass. *J. Amer. Cer. Soc.*, **37**, 370—378.

Rivers, M. L. & Carmichael, I. S. E. (1987): Ultrasonic studies of silicate melts. *J. Geophys. Res.*, **92**, 9247—9270.

Ryan M. P. & Blevins, J. Y. K. (1987): The viscosity of synthetic and natural silicate melts and glasses at high temperatures and 1 bar (10^5 pascals) pressure and higher pressures. *USGS Bull.* **1764**, 563 pp.

Sato, H. & Manghnani, M. H. (1985): Ultrasonic measurements of V_P and Q_p: relaxation spectrum of complex modulus on basalt melts. *Phys. Earth Planet. Int.*, **41**, 18—33.

Schaeffer, H. A. (1984): Diffusion-controlled processes in glass forming melts. *J. Non-Cryst. Sol.*, **67**, 19—33.

Schaeffer, H. A. & Muehlenbachs, K. (1978): Correlations between oxygen transport phenomena in noncrystalline silica. *J. Mater. Sci. Lett.*, **13**, 1146—1148.

Scherer, G. W. (1984): Use of the Adam-Gibbs equation in the analysis of structural relaxation. *J. Amer. Cer. Soc.*, **67**, 504—511.

— (1986): Relaxation in Glass and Composites. Wiley, New York, 331 pp.

Seddon, E., Tippet, E. J., Turner, W. E. S. (1932): *J. Soc. Glass. Techn.*, **16,** 450.
Seifert, F. A, Mysen, B. O., Virgo, D. (1981): Structural similarity between glasses and melts relevant to petrological processes. *Geochim. Cosmochim. Acta,* **45,** 1879—1884.
Shaw, H. R. (1972): Viscosities of magmatic silicate liquids: an empirical method of prediction. *Amer. J. Sci.,* **272,** 870—893.
Shimizu, N. & Kushiro, I. (1984): Diffusivity of oxygen in jadeite and diopside melts at high pressures. *Geochim. Cosmochim. Acta,* **48,** 1295—1303.
Silver, L. A. (1988): Water in silicate glasses. Ph. D. Thesis, Cal. Tech., 238 pp.
Simmons, J. H., Mohr, R. K., Montrose, C. J. (1982): Non-Newtonian viscous flow in glass. *J. Appl. Phys.,* **53:** 4075—4080.
Simmons, J. H., Ochoa, R., Simmons, K. D., Mills, J. J. (1988): Non-Newtonian viscous flow in soda-lime-silica glass at forming and annealing temperatures. *J. Non-Cryst. Sol.,* **105,** 313—322.
Spera, F. J., Borgia, A., Strimple, J., Feigenson, M. (1988): Rheology of melts and magmatic suspensions I. Design and calibration of concentric cylinder viscometer with application to rhyolitic magma. *J. Geophys. Res.,* **93,** 10273—10294.
Stolper, E. M. (1982a): Water in silicate glasses: An infrared spectroscopic study. *Contrib. Mineral. Petrol.,* **81,** 1—17.
— (1982b): The speciation of water in silicate melts. *Geochim. Cosmochim. Acta,* **46,** 2609—2620.
Sucov, E. W. (1963): Diffusion of oxygen in vitreous silica. *J. Amer. Cer. Soc.,* **46,** 14—20.
Tauke, J., Litovitz, T. A., Macedo, P. B. (1968): Viscous relaxation and non-Arrhenius behavior in B_2O_3. *J. Amer. Ceram. Soc.,* **51,** 158—163.
Tool, A. Q. & Eichlin, C. G. (1931): Variations caused in the heating curves of glass by heat treatment. *J. Amer. Cer. Soc.,* **14,** 276—308.
Watson, E. B., Sneeringer, M. A., Ross, A. (1982): Diffusion of dissolved carbonate in magmas: experimental results and applications. *Earth Planet. Sci. Lett.,* **61,** 346—358.
Webb, S. L. & Dingwell, D. B. (1990a): Non-Newtonian viscosities of geologic melts at high stresses: experimental results for rhyolite, andesite, basalt and nephelinite. (in press — *J. Geophys. Res.*)
— — (1990b): Onset of non-Newtonian rheology of silicate melts: A fiber elongation study. *Phys. Chem. Mineral.,* **17,** 125—132.
Williams, E. L. (1965): Diffusion of oxygen in fused silica. *J. Amer. Cer. Soc.,* **48,** 190—194.
Wong, J. & Angell, C. A. (1976): Glass structure by spectroscopy. Dekker, New York, 864 pp.

Received 5 October 1989
Accepted 8 February 1990